

A physics-based probabilistic forecasting model for rainfall-induced shallow landslides at regional scale

Shaojie Zhang^a, Luqiang Zhao^b, Ricardo Delgado-Tellez^c, Hongjun Bao^b

^aKey Laboratory of Mountain Hazards and Earth Surface Process, Institute of Mountain Hazards and Environment, Chinese Academy of Sciences, Chengdu 610041, China;

^bPublic Meteorological Service Center of CMA, China Meteorological Administration, Beijing 100081, China

^cNipe Sagua Baracoa mountain office, Ministry of Science, Technology and Environment of Cuba, Guantanamo, Cuba

Correspondence to: L.Q. Zhao (zhaolq@cma.gov.cn)

Abstract: Conventional outputs of physics-based landslide forecasting models are presented as deterministic warnings by calculating the safety factor (F_s) of potentially dangerous slopes. However, these models are highly dependent on variables such as cohesion force and internal friction angle which are affected by high degree of uncertainty especially at a regional scale, which result in unacceptable uncertainties of F_s . Under such circumstances, the outputs of physical models are more suitable if presented in the form of landslide probability values. In order to develop such models, a method to link the uncertainty of soil parameter values with landslide probability is devised. This paper proposes the use of Monte Carlo method to quantitatively express uncertainty by assigning random values to physical variables inside a defined interval. The inequality $F_s < 1$ is tested for each pixel in n simulations which are integrated in a unique parameter. This parameter links the landslide probability to the uncertainties of soil mechanical parameters and is used to create a physics-based probabilistic forecasting model for rainfall-induced shallow landslides. The prediction ability of this model was tested in a case study, in which simulated forecasting of landslide disasters associated to heavy rainfalls on July 9 of 2013 in the Wenchuan earthquake region of Sichuan province, China was performed. The proposed model successfully forecasted landslides in 159 of the 176 disaster points registered by the geo-environmental monitoring station of Sichuan province. Such testing results indicate that the new model can be operated in a high efficient way and show more reliable results attributing to its high prediction accuracy. Accordingly, the new model can be potentially packaged into a forecasting system for shallow landslides providing technological support for the mitigation of these disasters at regional scale.

Keywords: Landslide, probabilistic forecasting, infinite slope model, hydrological process simulation

1 Introduction

Rainfall-induced shallow landslides are common in many mountainous areas and are considered extremely dangerous (Varnes, 1978). In despite the low volume of debris deposits involved in these processes (generally $< 1,000 \text{ m}^3$), rainfall-induced shallow landslides present high moving speeds (Cruden and Varnes, 1996), evolve very rapidly, and can propagate even in presence of obstacles (Davide T. and Davide R., 2010). Current regional landslide forecasting models mainly focuses on shallow landslides. They can be classified in three categories: statistics-based methods (Caine, 1980; Crosta, 1998; Crosta and Frattini, 2001; Aleotti, 2004; Wei et al., 2004; Wieczorek and Glade, 2005; Cardinali et al., 2006; Jacob et al., 2006), contributor-factor-based forecasting methods (Dai and Lee 2003; Wei et al., 2007a; Chang et al. 2008) and physics-based forecasting methods (Montgomery and Dietrich, 1994; Wu and Sidle, 1995; Montgomery et al., 1998; Iverson, 2000; Wilkinson et al., 2002; Crosta and Frattini, 2003; Salciarini et al., 2006). The physics-based forecasting models have overcome the drawback of statistics-based models with respect to excessive dependence on rainfall data. Furthermore, by devising mechanisms for coupling rainfall with soil surface mechanics using hydrological process simulation (Zhang et al., 2014a), the physically-based models represent an improvement over the independent treatment of these factors by contributor-factor-based forecasting models e.g. (Wei et al., 2007a).

The physics-based forecasting model is able to describe the variation rule of hydrological parameters induced

by rainfall infiltration and further explain the failure mechanism of a slope due to the variation of hydrological parameters. Those characteristics explain the interest of scholars to the physics-based forecasting model and its implementation at regional scales (Schmidt et al., 2008; Montrasio et al., 2011; Raia et al., 2014). The most common analysis unit used in physics-based forecasting models is the pixel, used for example in the well-known TRIGRS model (Baum, et al., 2002, 2008). The safety factor of each pixel within a forecasting region, F_s ($F_s=R/S$: where R is shear resistance and S is the driving force) is calculated considering rainfall infiltration, pixels are then identified as unstable ($F_s > 1$) or stable ($F_s < 1$). From these results, landslide warnings are expressed deterministically by labeling each pixel of the forecasting area as either ‘landslide occurrence’ or ‘nonoccurrence’.

However, it must be noted that the underlying physics-based forecasting model requires large number of surface data to be assigned to each pixel before safety factors can be calculated. The physics-based model is sensitive to the accuracy of such data, especially the soil mechanical parameters (cohesion force and internal friction angle) that can significantly influence the pixel stability. In general, and specially for large areas, seemingly deterministic soil mechanical parameters at pixel level used in physical models have different amounts of uncertainty (Schmidt et al., 2008; Rossi et al., 2013), which thus generate uncertain forecasting results. In this scenario, it is unwise to give deterministic forecasting results to the public while using the physical model in local forecasting service.

Providing probabilistic landslide forecasting results is the more direct solution to this issue. Currently, several scholars advance in the development of physics-based probabilistic forecasting models (Schmidt et al., 2008; Raia et al., 2014). However, the relationship between the landslide probability and the uncertainties in soil mechanical parameters is not addressed in their models. This effectively renders such probabilistic models actually still in deterministic mode. For example, in Raia et al. (2014) a series of deterministic forecasting results are generated by the model during the simulation process from which an experienced forecaster with professional knowledge of landslides is necessary for picking up the most probable one. Consequently, this approach requires a large number of calculations, which is unsuitable for operational forecasting of shallow landslides.

This paper focuses on an effective method for linking landslide probability to the uncertain soil mechanical parameters. It uses Monte Carlo methods to propose a probabilistic forecasting model with a high calculating efficiency. The proposed model can directly generate probabilistic forecasting results instead of serial of deterministic results, and hence it will be more suitable to operational forecasting of shallow landslides, in special at the regional scale.

The next section introduces the physics-based probabilistic forecasting for shallow landslides model. Third section addresses the general aspects of its application to a regional scale shallow landslide forecasting system. Fourth section describes a case study in which the effectiveness of the proposed model is analyzed in a study case. Sections five and six discuss the results and states the conclusions of this study respectively.

2 Probabilistic forecasting for shallow landslides

2.1 The Infinite slope model for unsaturated soil slopes using safety factor F_s

There are two mechanisms that trigger failure in slopes subject to rainfall infiltration. They are loss of matrix suction and increasing of a positive pore water pressure (Li et al., 2013). In southwestern China, precipitation is rich in summer due to monsoon conditions from both Pacific and India Ocean (Wei et al., 2006). Before of the raining season slopes in this area are generally unsaturated during the relatively dry seasons. Almost all landslide disasters in southwestern China occur during the rainy season when the matrix suction of topsoil’s suddenly decreases due to monsoon heavy rains. Consequently, this research focuses on the stability analysis of unsaturated soil mass.

During the evolution process from stability to failure driven by rainfall infiltration, the rapid loss of suction due to the increasing soil water content is the key triggering factor for shallow landslides. The safety factor F_s is used to evaluate the stability of slopes under the action of rainfall infiltration; in this scenario, the failure plane is

governed by the Mohr-Coulomb failure criteria of unsaturated soil mass, and is assumed to be parallel to the slope surface (Fig.1). The expression of F_s based on the shear strength formula of the unsaturated soil (Fredlund and Rahardjo, 1993) and the infinite slope model can be expressed as follows:

$$F_s = \frac{\tan \varphi}{\tan \beta} + \frac{c + \psi \tan(\varphi^b)}{\gamma_t H_s \cos \beta \sin \beta} \quad (1)$$

Where c is a stress and can be named of the cohesion force, φ is the internal friction angle, φ^b is related to the matrix suction (which is close to the internal friction angle φ in the condition of the low matrix suction), H_s is the soil depth, ψ is the matrix suction of the soil, which is a function of the soil water content described as follows (Van Genuchten, 1980):

$$S_e = \frac{\theta - \theta_r}{\theta_s - \theta_r} = \left[\frac{1}{1 + (\alpha \times \psi)^n} \right]^m \quad (2)$$

where S_e is the saturation degree, θ_s is the saturated water content, θ_r is the residual water content, θ is the soil water content of the current hour, α , n and m are the parameters of soil-water characteristic curve, and $n=1-1/m$.

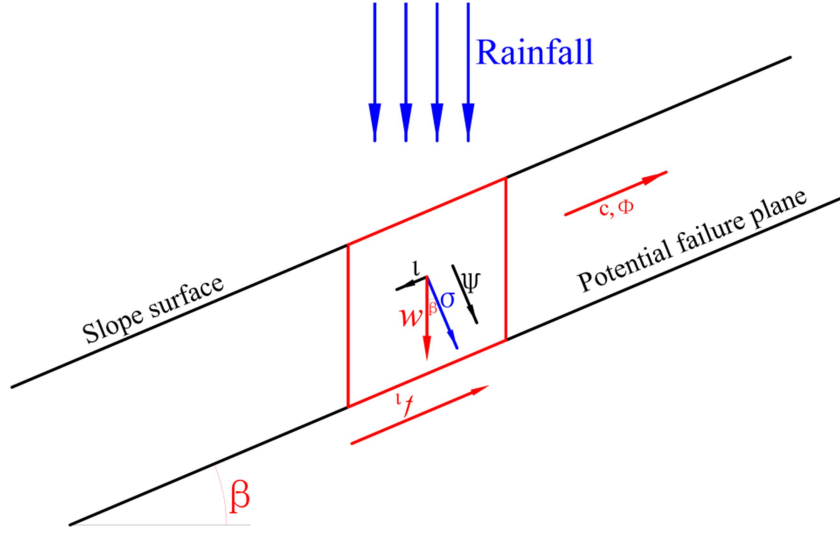


Fig.1 Infinite slope model for unsaturated soil in a slope

2.2 Deterministic forecasting model using safety factor F_s

The infinite slope model aims to calculate the safety factor F_s to identify the stability of a slope. It has its basis in a theoretical hypothesis (Apip et al., 2010), which can describe the mechanical process of shallow landslides formation. This approach can give reliable results for each pixel as long as the soil mechanical parameters are accurate. From a deterministic point of view, this physical framework can be briefly drawn as follows: for each pixel in the forecast area, if $F_s \leq 1$ it's considered unstable, while pixels with $F_s > 1$ are considered to be stable.

Acquiring the values for the soil mechanical parameters necessary for the infinite slope model require the use of field sampling or soil-texture based methods (Blondeau, 1973; Apip et al., 2010; Zhang et al., 2014a; Zhang et al., 2014b). However, the precision of these methods are relatively low (Schmidt et al., 2008), thus subject to high levels of uncertainty. Consequently, the seemingly deterministic infinite slope model based on soil mechanical parameters of each pixel is in fact uncertain (Schmidt et al., 2008; Rossi et al., 2013). This will be reflected in the safety factors F_s of each pixel, leading to a situation in which, despite the advantages of the physical-based landslide forecasting model, it may be misleading if used in a deterministic way for real world applications.

This is not an issue for other landslide forecasting models. For example, although the input variables of the contribution-factors-based forecasting model are also uncertain (Wei et al., 2007a) and thus it essentially belong to

statistical models (Zhang et al., 2014a) it successfully account for the relationship between uncertainties of input variables and results using fuzzy mathematics so that they are expressed as probabilistic forecasting for landslides. The landslide probability is divided into five grades from 1st to 5th level, which represents a low, relative low, medium, high and extremely high probability of occurrence of landslides, respectively. This forecasting result conveys clearer landslide risk levels to the public (Wei et al., 2007b).

Due to the above reasons it is relevant to identify an effective relationship between the landslide probability and uncertain input variables with uncertainty (cohesion force and internal friction angle) in a physics-based probabilistic forecasting model.

2.3 Probabilistic forecasting model for shallow landslides

In order to link landslide probability to uncertain variables, the nature of this uncertainty should be quantitatively expressed in mathematical language. Then, a physical parameter associated with both, input variables and landslide probability will be used to formalize the linkage.

The uncertainty of physical parameters can be described by a probability density function (Schmidt et al., 2008), because the uniform distribution suited in the investigation of large areas where information on the geo-hydrological properties is limited (Raia et al., 2014), which can easily allow authors to get random parameters from its set approximate variation range instead of large amount of field and experimental works in large area. Accordingly, the uncertainties of cohesion force and internal friction angle are described here as uniform probability distributions in the intervals of $c=U(c_{min}, c_{max})$, and $\varphi=U(\varphi_{min}, \varphi_{max})$, respectively. Then, Monte Carlo method can be used to randomly extract cohesion force and internal friction angles from the two intervals n times in any forecasting step. This random approach is used to account for the uncertain nature of soil mechanical parameters. The detailed description of random extracting process is as follows: the extraction of the two parameters is dependent on the variable r_i which is described as uniform probability distributions in the interval of $r_i=U(0,1)$, the random values of cohesion force c_i and internal friction angle φ_i can be identified via Eq. 3 and Eq.4. In these equations, r_i can help to get a random number c_i with uniform distribution rule between c_{min} and c_{max} , because the variable r_i submits this distribution rule between 0 and 1.

$$c_i = r_i(c_{max} - c_{min}) + c_{min} \quad (3)$$

$$\varphi_i = r_i(\varphi_{max} - \varphi_{min}) + \varphi_{min} \quad (4)$$

There, c_{min} and φ_{min} are lower borders of intervals of the two mechanical parameters expected values; c_{max} and φ_{max} are the upper borders. For any pixel in any forecasting step, a matrix M_i can be generated after the n -times random extraction process:

$$M_i = [c_i, \varphi_i] = \begin{bmatrix} c_1 & \varphi_1 \\ c_2 & \varphi_2 \\ c_3 & \varphi_3 \\ \dots & \dots \\ c_n & \varphi_n \end{bmatrix} \quad (5)$$

Any element contained in M_i has a specific physical meaning representing as a whole the physical phenomenon of uncertainty.

Provided other parameters identified in Eq. 1, each set of $[c_i, \varphi_i]$ in M_i can generate a safety factor $FS_i = [FS_1, FS_2, FS_3, \dots, FS_n]$. The array of safety factors FS_i reflects n possible stable states for a pixel under these physical conditions. It's possible from there to identify a failure probability by the number of $FS_i \leq 1$ (failure) in the n different states in the form of a ratio P ($P \in [0,1]$) of $FS_i \leq 1$ representing a tendency of a pixel to failure from stability.

$$P = \frac{\text{Sum}_{FS < 1}}{n} \quad (6)$$

Larger P values in Eq. 6 indicates a forecasting result favorable to a high occurrence probability of failure under uncertain variables. This interpretation implies that a pixel will tend to one end failure when P exceeds 50% and its failure probability will only increase with larger values of P . Since P is derived from series of random (uncertain) variables $[c_i, \varphi_i]$ via Eq.1 and Eq. 6, and is also directly associates with the landslide probability, the ratio ($P \in [0,1]$) of $Fs_i \leq 1$ is a strong candidate for linking the landslide probability to the uncertain soil mechanical parameters.

For the purposes of practical implementation of this forecasting model, P is divided into a series of reference intervals in Table 1, the occurrence probability of shallow landslides increase from 1st interval to 5th interval of P . Five grades of landslide warnings are defined accordingly and color-coded Table 1.

Table 1 Reference intervals for shallow landslides forecasting based in probabilistic safety factor

| Ratio intervals/% | $P < 20$ | $20 \leq P < 50$ | $50 \leq P < 60$ | $60 \leq P < 80$ | $80 \leq P < 100$ |
|-------------------|-----------|------------------|------------------|------------------|-------------------|
| Warning degree | 1 | 2 | 3 | 4 | 5 |
| Warning color | Colorless | Blue | Yellow | Orange | Red |

3 Probabilistic shallow landslides forecasting method at regional scale

3.1 Gathering basic data necessary for landslide forecasting

Topography is the main factor in shallow landslides. Nowadays, obtaining a DEM of precision adequate for regional scale forecasting is straightforward. The DEM of the study zone is re-sampled into pixels with dimensions according to the extension of the area. The parameters required to calculate the ratio P for each pixel from the array of safety factors Fs_i from a series of randomly extracted $[c_i, \varphi_i]$ are identified in Eq.1. In this case matrix suction, which is associated with the soil water content, should be identified by hydrological process simulation.

The key data necessary for the hydrological process simulation include the spatial distribution of precipitation, land use, soil type and NDVI. Precipitation data with the same solution of the DEM can be obtained by re-sampling rainfall prediction from Doppler radar supplied by meteorological bureaus. Land use, soil type and soil depth can be obtained from corresponding databases, all of which should be transformed into grid data with the same solution of DEM. Other data necessary for stability calculations are slope angle for each pixel, parameters from soil-water characteristic curve (α, m, n), and soil mechanical parameters. Slope angles can be derived from DEM using spatial analyst tools, parameters (α, m , and n) of the soil-water characteristic curve are derived from the different soil types within the pixel.

Regarding the identifications of soil mechanical parameters (cohesion force and internal friction angle), a relatively reliable way such as field sampling or soil-texture based methods should be used to assign an initial basic value to each pixel. Although these values include high uncertainty levels, they are used only as reference values while setting intervals of $c=U(c_{min}, c_{max})$, and $\varphi=U(\varphi_{min}, \varphi_{max})$ (Raia et al., 2014). In this study, the lithology of the study zone is derived from a geological map, and the mechanical parameters (cohesion force and internal friction angle) of the corresponding lithology are identified using a rock mechanics handbook (Ye et al., 1991). Finally the data is assigned to each pixel using the grid cells of the DEM as reference.

From Eq.3 and Eq.4, it is necessary to identify the lower and upper border of intervals of the soil mechanical parameters. However, the exact values for lower (c_{min} and φ_{min}) and upper (c_{max} and φ_{max}) limits are very difficult to determine. From currently published papers, there is no known theoretical or experimental method to solve this issue. Raia et al. (2014) used variations of 1%, 10% and 100% around the values of cohesion force and internal friction angle (from field tests) to get several intervals, showing that the forecasting effectiveness is significantly improved by using a large variations. Consequently, this method applies a variation of 100% around the mean value of these parameters for each pixel to set the corresponding lower and upper borders as follows:

$$c_{\text{random}} \in [0.5 \times c_{\text{origin}}, 2 \times c_{\text{origin}}] \quad (7)$$

$$\varphi_{\text{random}} \in [0.5 \times \varphi_{\text{origin}}, 2 \times \varphi_{\text{origin}}] \quad (8)$$

Where c_{random} and φ_{random} are the randomly extracted cohesion forces and internal friction angles, c_{origin} and φ_{origin} are the mean value of each pixel (in this case from the rock mechanics handbook (Ye et al., 1991)).

3.2 Pixel level hydrological process simulation

The simulation of hydrological processes including rainfall interception, infiltration, and evapotranspiration is extremely complicate. However, rainfall infiltration is the key factor in the distribution of soil water content in underlying surface which simplify the analysis. In southwestern region of China slopes are almost unsaturated before the rainy season due to characteristic distribution of rainfall influenced by monsoon (Zhang et al., 2014b). The infiltration process in the vertical direction in unsaturated soil mass can be described by the 1D Richards's equation (1931):

$$\frac{\partial \theta}{\partial t} = \frac{\partial}{\partial z} \left[D(\theta) \frac{\partial \theta}{\partial z} \right] - \frac{\partial K(\theta)}{\partial \theta} \quad (9)$$

Where θ is soil water content, $D(\theta)=K(\theta)/(d\theta/d\psi)$ is the hydraulic diffusivity, ψ is the suction of unsaturated soil, z represents the soil depth, which is positive along the soil depth and have the topsoil as the origin point, $K(\theta)$ is the hydraulic conductivity. The matrix suction is the dominant external force to drive the water movement in unsaturated soil mass, which can be calculated from Eq. 2.

Infiltration upper border: If the topsoil is unsaturated, it has a strong infiltration capacity (Lei et al., 1988). Then, while the rainfall intensity is less than the infiltration capacity of the topsoil, all precipitation will infiltrate into topsoil without any runoff. In this scenario, the infiltration border is governed by Eq. (10):

$$-D(\theta) \frac{\partial \theta}{\partial z} + K(\theta) = R(t), \quad t > 0, z = 0 \quad (10)$$

Where $R(t)$ is the rainfall intensity at time t . Here, the part of precipitation that exceeds the capacity of infiltration of the topsoil will transform into runoff (no water storage above topsoil). In this case the topsoil of a pixel is considered saturated. Thus, the Eq.10 that governs infiltration upper border is transformed into the equation of $\theta=\theta_s$ (Lei et al., 1988). There θ_s is the saturated moisture corresponding to the soil type.

Infiltration bottom border: It has been experimentally demonstrated that the soil water content beyond a soil depth of 40 cm is barely influenced by rainfall infiltration (Cui et al., 2003). Consequently a region with a groundwater level near the surface of the soil has hydrological characteristics in which rainfall infiltration can hardly induce any groundwater level variation. In this case, it is reasonable to ignore the water exchange process between the lower boundary and groundwater (Zhang et al., 2015).

An implicit finite difference method is used for discretization of the 1D differential equation of water movement. The calculation time t is segmented into several intervals with the same time gap Δt , and the soil depth L of each pixel is segmented into soil layers (each layer is named of i number) with the same depth Δz .

Identifying the initial soil water content is an important issue during the hydrological simulation process. However, this value cannot be directly determined at any given time for a large region due to complex rainfall infiltration and evapotranspiration interactions. In the case of southwestern China, the winter is generally a relatively dry season thus; the soil water content value of the topsoil is very low, close to the residual water content of the soil type (Zhang et al., 2014b). This situation is exploited setting the simulation time to start on January 1 of the forecasting year (driest month in winter), which allows the use of the residual water content corresponding to the soil type as and the initial value of the topsoil water content. Measured meteorological data from January 1 are then feed to the simulation, which allows for a relatively accurate initial value of soil water content for the landslide forecasting. Each simulation step takes also into account the rainfall interception and evapotranspiration processes by means of the algorithm of distributed hydrological model GBHM (Yang et al., 2002).

After the hydrological simulation process identify the initial soil water content of each pixel, the simulation focuses on the extraction of key hydrological parameters (soil water content and matrix suction) necessary for the

238 stability calculation of each pixel using the expected rainfall from Doppler radar forecasting. During this last stage
 239 in the simulation in which landslide forecasting is performed, the evapotranspiration processes is not considered
 240 since this period is typically short, with rainfalls, negligible sunshine and lower temperatures.

241 3.3 Probabilistic landslide forecasting at pixel level

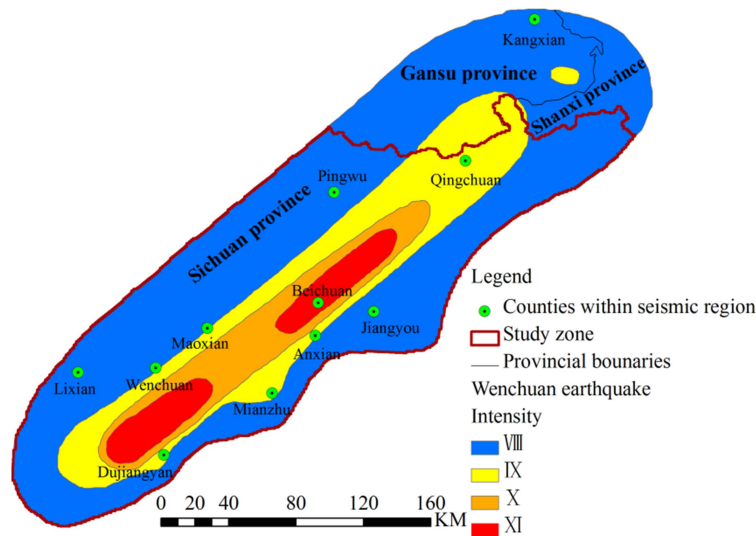
242 During the forecasting stage, the hydrological parameters (soil water content and matrix suction) of each pixel
 243 in each forecasting step Δt are extracted via hydrological process simulation. Then the ratio P is computed for
 244 each pixel in several steps as follows: (1) The Monte Carlo method is used to extract the cohesion force and the
 245 internal friction angle n times from the corresponding intervals ($c=U(c_{min}, c_{max})$, and $\varphi=U(\varphi_{min}, \varphi_{max})$) of each pixel;
 246 (2) The safety factor F_s of each divided layer within one pixel is calculated after each extraction, using the soil
 247 mechanical parameters and the hydrological parameters only related to time as inputs of Eq.2, when the F_s of i^{th}
 248 layer is less than 1, then the calculation process within the pixel will stop; (3) Once the Monte Carlo process end,
 249 the total times $Sum_{F_s < 1}$ of $F_s < 1$ is obtained, and the ratio P of $F_s < 1$ is calculated by Eq.6; (4) Finally the interval
 250 of Table 1 where ratio P is located according to its value is assigned to the pixel as the early warning information
 251 to be broadcasted.

252 After completing this process for all pixels within the forecasting region, the whole calculation at time t is fin-
 253 ished, meanwhile a map of landslide warning degrees in the forecasting region will be generated at the end of each
 254 forecasting step. Such maps can then be used by the forecasting bureau of the region to issue landslide warnings to
 255 hazard mitigation units and the public.

256 4 Verification of the probabilistic landslide forecasting model

257 4.1 Study zone

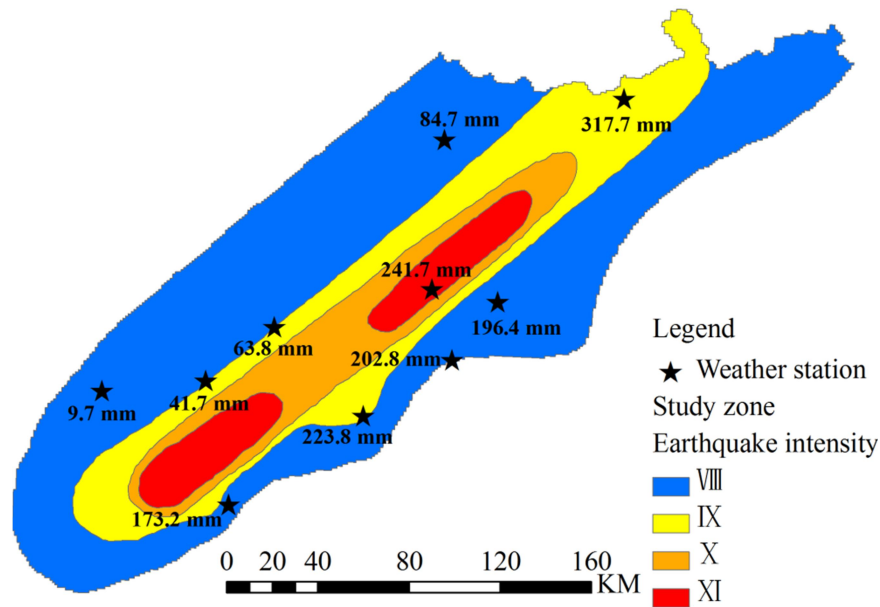
258 The Wenchuan earthquake region with an area $3.14 \times 10^4 \text{ km}^2$ within Sichuan province, China is chosen as the
 259 study zone in this study (Fig.2). In this region, at 14:28 PM (Beijing time) on May 12rd 2008, an Ms 8.0 earth-
 260 quake occurred. Massive potential unstable slopes were left after this earthquake, which are known to readily
 261 evolve into shallow landslides by rainfall infiltration (Zhang et al., in Pres.). The close relationship between rain-
 262 fall and landslides in this region has been demonstrated by the short lag time of landslides and its strong correla-
 263 tion to rainfall time (Tang, 2010). The same study established that landslide events within the earthquake region
 264 are mainly in the form of shallow landslides (Tang, 2010). Tang (2010) also pointed out that shallow landslides
 265 will be active within Wenchuan earthquake region at least for the next ten years. Such conditions make this region
 266 ideal for implementation of shallow landslides forecasting models.



267 Fig.2 Study zone and intensity distribution of Wenchuan earthquake
 268

269 **4.2 Rainfall process and related landslide events used for testing**

270 The chain of events in the Wenchuan earthquake area that ended in disastrous landslides in July 9th of 2013
271 was chosen to evaluate the proposed landslide probabilistic forecasting method. These events started with heavy
272 rainstorms in the area during the days from July 1th to July 8th of 2013. As the rainfall measured by the weather
273 stations within the area shows (Fig.3), the maximum accumulated precipitation during these days reached 317.7
274 mm, which become a key contributing factor for the landslide events of July 9th of 2013.



275 Fig.3 Total rainfall from 1st to 7th of July 2013

277 On July 9th of 2013, there was no evidence of decreasing rainfall intensity, on the contrary all evidence sug-
278 gested heavier rainfalls. Records from the rainfall forecasted by Doppler radar provided by the weather bureau of
279 Sichuan province on that day, predicted a maximum 24-hour total precipitation within the earthquake region of up
280 to 498 mm (Fig.4). Accordingly, the Weather Bureau of Sichuan province published red color warning signals
281 (which are the highest alert degree) for some locations within the study region. On that day, 176 landslide events
282 were reported within the study region (Fig.4) leading to casualties and serious economic losses for local residents
283 (Zhang et al., 2014b). This typical landslide disaster triggered by intense rainfall is ideal to evaluate the main as-
284 pects of the implementation of the proposed probabilistic landslide forecast model at regional scales.

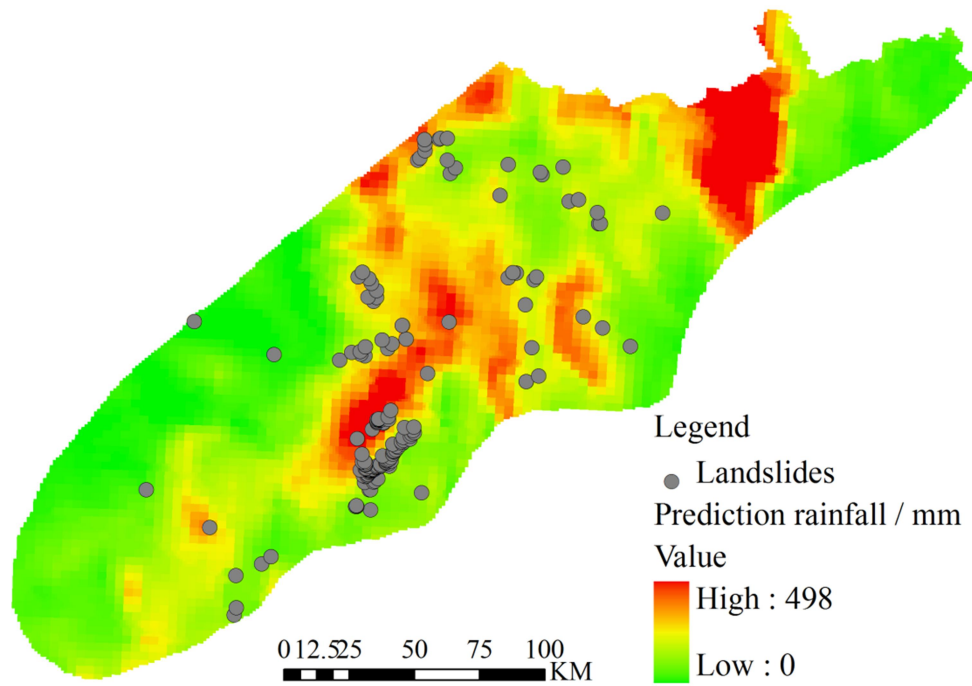


Fig.4 Distribution of rainfall-induced landslides within Wenchuan earthquake region on July 9th of 2013

4.3 Gathering of basic data of study zone

The topography of the study region (Fig.5) was described by 125 m \times 125 m DEM. This way, the study region was segmented into 6965505 pixels. A data matrix with 2576 rows and 2704 columns was created from the DEM and saved in text format. The basic data for hydrological process simulation and stability was resampled to correspond to the same resolution of the DEM and saved as text matrices with the same dimensions.

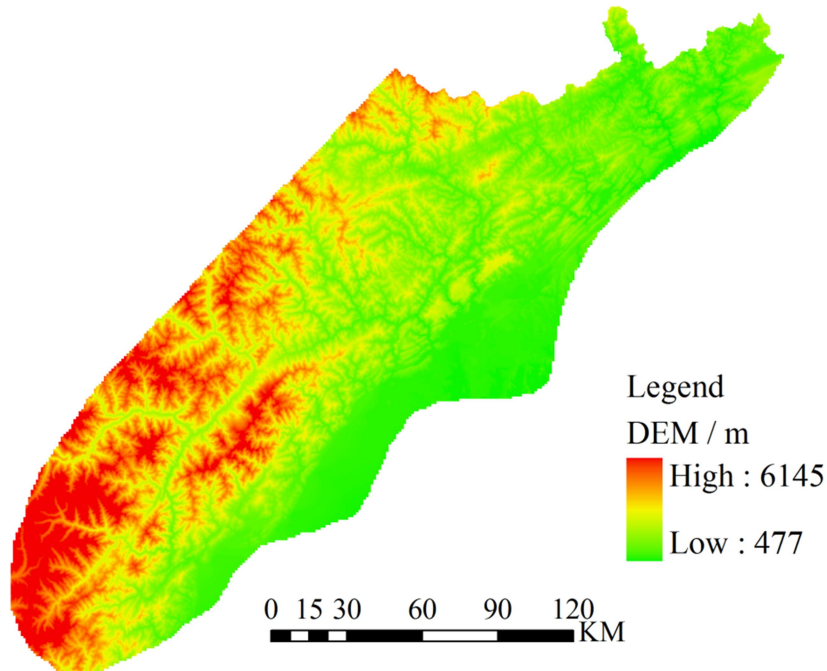


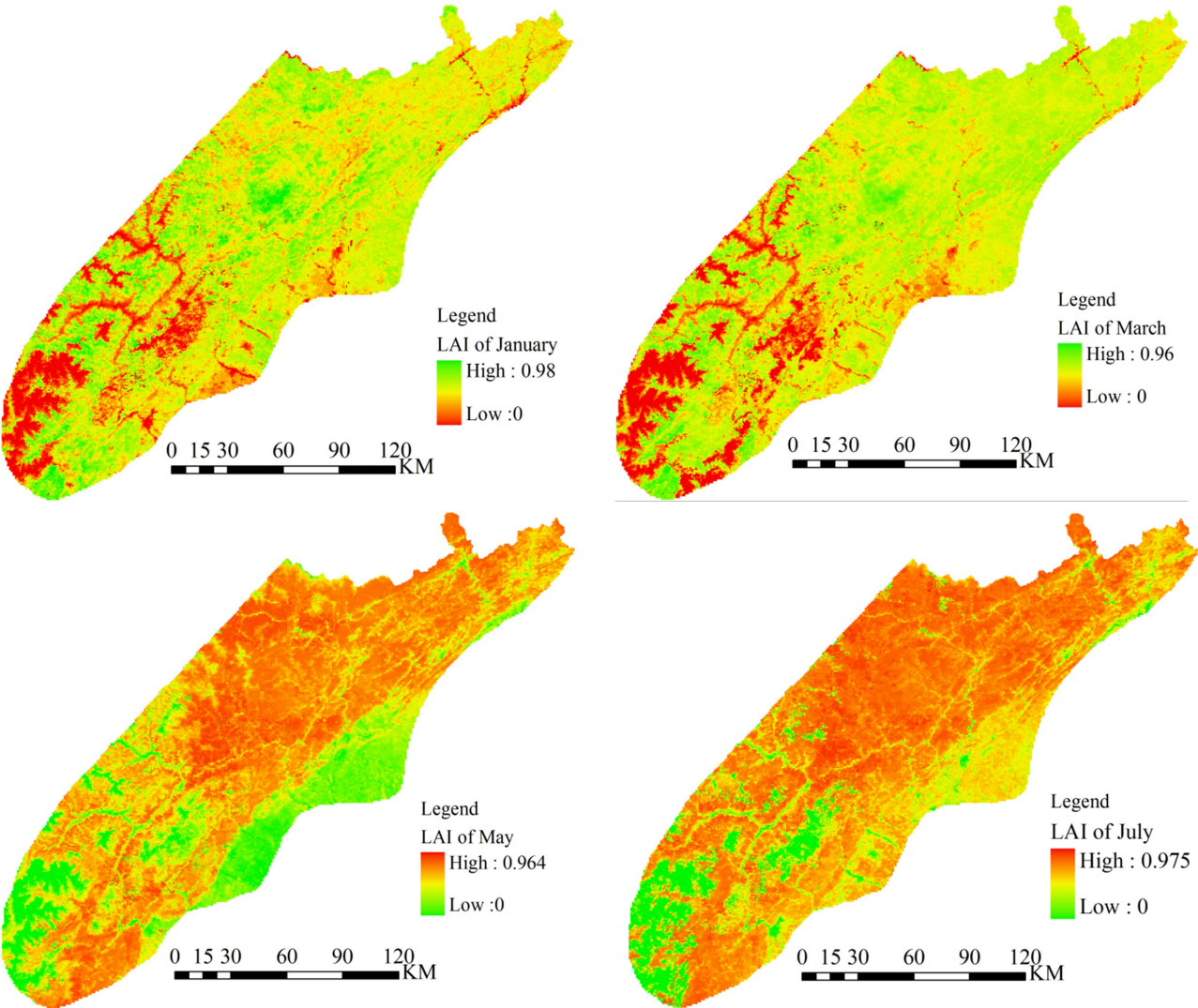
Fig.5 DEM of Wenchuan earthquake area

4.3.1 Data for hydrological process simulation

The process of rainfall interception due to vegetation influence within the study region is taken into account

296 using NDVI values. Generally, the vegetation, and thus the values of NDVI vary with the variation of land uses
 297 and seasons. In this case, NDVI values from the same reason of the adjacent year are considered reasonably close,
 298 since the distribution of land uses within a region is relatively stable. The monthly NDVI distribution over the
 299 study region in the precedent year (2012) was used to adjust for canopy rainfall interception during the hydrolog-
 300 ical process simulation (Fig.6).

301



302

303 Fig.6 Distributions of the LAI within the study zone

304 Other data required, such as land use (Figure 7 (a)), soil type (Figure 7 (b)), and the soil depth for Wenchuan
 305 earthquake region was obtained from the FAO database (<http://www.fao.org/geonetwork/srv/en/main.home>). The-
 306 se data was processed using GIS functions so that they correspond to the pixels of the DEM.

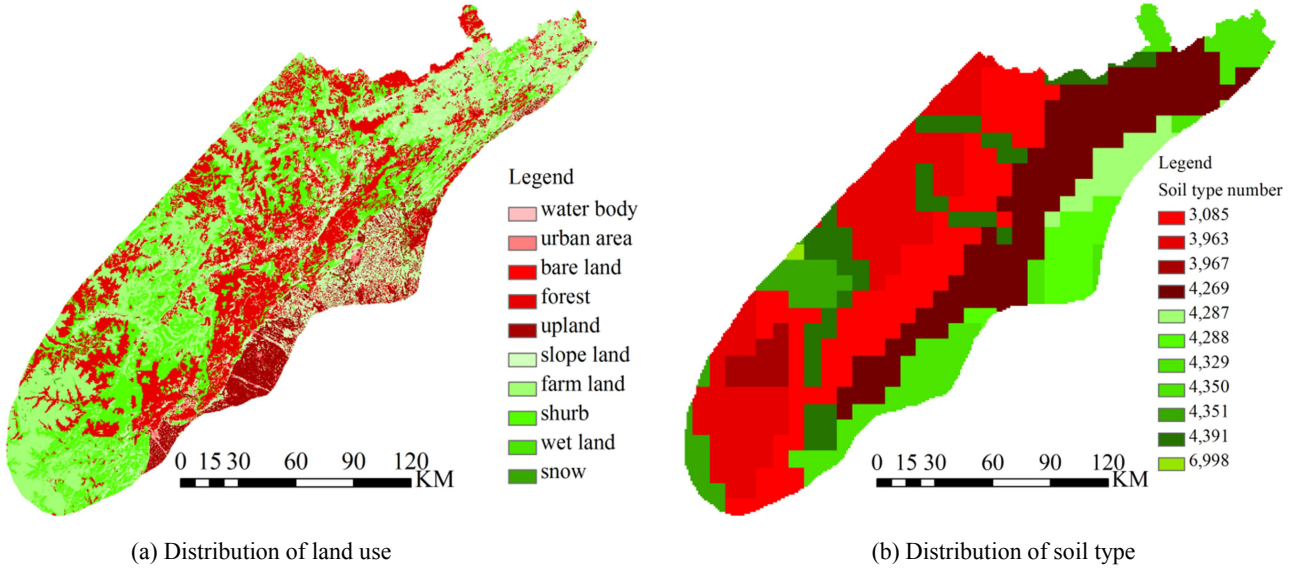


Fig. 7 Information of land uses and soil types within the study zone

The physical parameters of the soil required for the simulation of rainfall infiltration in the vertical direction were determined by the land use and standard soil types within the study region. The soil thickness ranged from 1 to 4 m, soil depths of 1 m accounts for 44.1% of the study area, while deeper soils cover the remaining 55.9%. Each pixel was divided into 10 layers (along the soil depth in the vertical direction) during the discretization process. There are 10 soil types in the area (shown in Fig. 7b). Their relevant physical properties are listed in Table 2.

Table2 Soil-water parameters for hydrological simulation

| Soil type code | Saturated moisture | Residual moisture | Parameters of curve | | Saturated hydraulic conductivity(mm/h) |
|----------------|--------------------|-------------------|---------------------|----------|--|
| | | | <i>Alpha</i> | <i>n</i> | |
| 3085 | 0.48278 | 0.07768 | 0.01896 | 1.40474 | 22.78608 |
| 3963 | 0.47303 | 0.07347 | 0.01796 | 1.42367 | 22.46508 |
| 3967 | 0.52726 | 0.08259 | 0.01867 | 1.41453 | 35.97075 |
| 4269 | 0.45649 | 0.06905 | 0.02306 | 1.55872 | 32.68625 |
| 4287 | 0.44596 | 0.07343 | 0.01971 | 1.47235 | 19.30871 |
| 4288 | 0.43797 | 0.07175 | 0.02064 | 1.53067 | 24.80996 |
| 4329 | 0.45049 | 0.07957 | 0.01604 | 1.44517 | 9.307170 |
| 4350 | 0.47990 | 0.07435 | 0.02156 | 1.42176 | 22.51646 |
| 4351 | 0.48278 | 0.07723 | 0.02040 | 1.41974 | 21.61279 |
| 4391 | 0.42784 | 0.06439 | 0.01623 | 1.63524 | 23.91267 |
| 6998 | 0.46154 | 0.06817 | 0.01770 | 1.46884 | 23.60925 |

4.3.2 Data for calculation of slope stability

The Eq.1 indicates that matrix suction, cohesion force, and internal friction angle are the key mechanical parameters influencing the slope stability. Simulation of the hydrological process is used to obtain the matrix suction of soil mass as a function of the soil water content as shown in Eq. 2. Cohesion forces and internal friction angles for each pixel updated from the old database (Liu et al., 2016) are determined according to lithology map and the rock mechanical handbook (Fig.8), the detailed process to obtain these data are as follows: each pixel will be firstly assigned the lithology attribution according to the lithology map, and then the rock mechanical handbook which contains the mechanical parameters of all lithology will be used to find the corresponding parameters of each pixel. These mechanical values are then used as a basic reference for constructing intervals of these parameters ($c=U(c_{min}, c_{max})$, and $\varphi=U(\varphi_{min}, \varphi_{max})$) for each pixel.

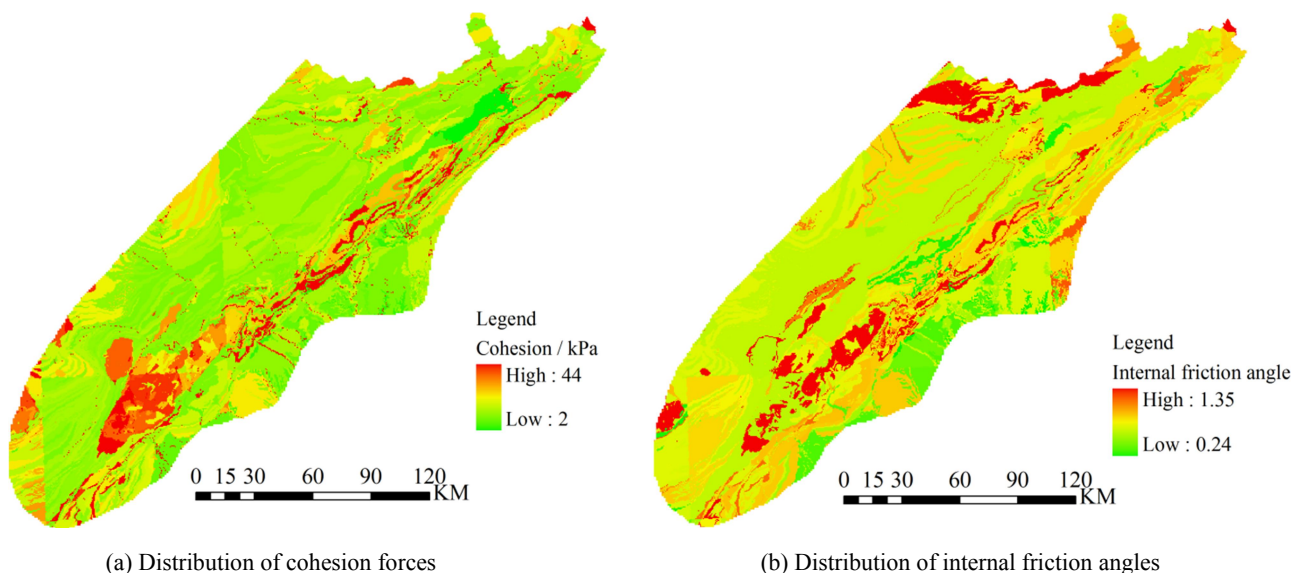


Fig.8 Mechanical paramters of soil used for calculation of slope stability

4.4 Forecasting results

The landslide probability in Wenchuan earthquake region on July 9, 2013 was calculated, along with color-coded warnings for each pixel according to Table 1. This forecast covered 24 time nodes (hourly forecasts) covering the whole day. Two representative time nodes (at 6:00 AM and 15:00 PM) are chosen from the 24 h forecasting results for further analysis (figure 9). The detailed forecasting results are listed in Table 3. These details denote low variation in the forecast for these time nodes.

Table 3 Quantity of pixels with warning information

| | | Blue | Yellow | Orange | Red |
|-------|----------|------|--------|--------|-----|
| pixel | 6:00 AM | 534 | 150 | 332 | 699 |
| count | 15:00 PM | 527 | 158 | 321 | 704 |

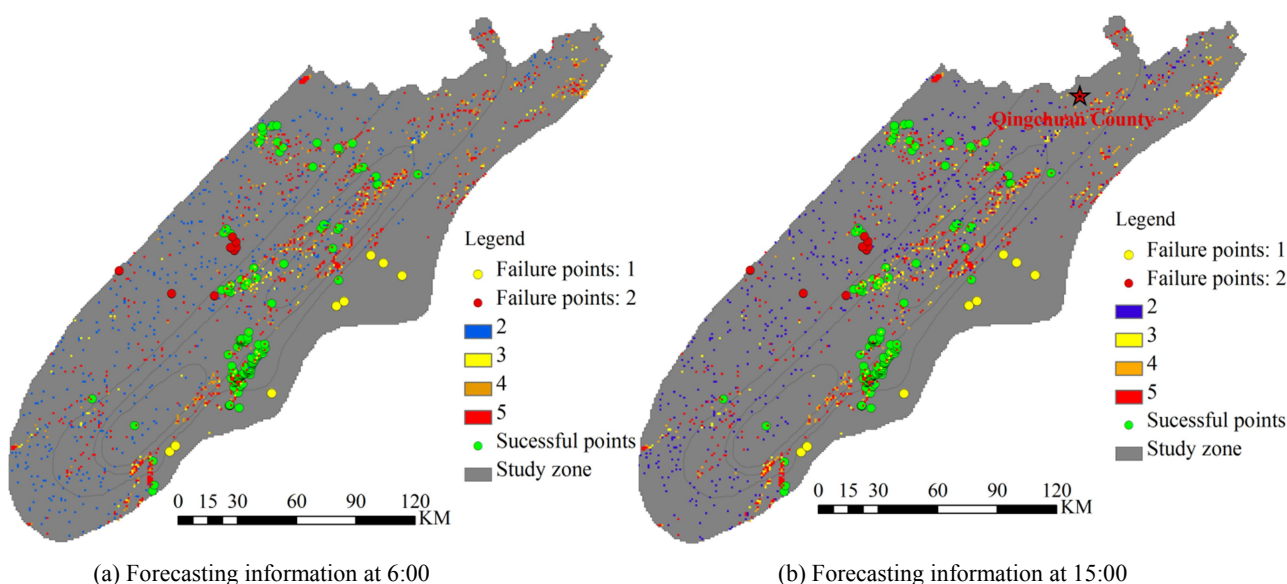


Fig.9 Landslide warning maps for Wenchuan earthquake region at two representative time nodes.

Colored points in fig. 9 represent landslide disasters occurred on July 9, 2013. Green points represent landslides located in pixels forecasted with high degree of probability of landslides (orange-red), thus they are considered successfully forecasted or true positives (159 events). The other 17 events represented by yellow and red

points denote landslide events in low warning areas, which are considered as failed-forecasted landslides or false negatives. These numbers indicate a missing-prediction rate of the new proposed forecasting model of about 9.7%.

Further analysis of these failures indicated that in some cases, the maximum slope angle of the corresponding pixel reported by the DEM is less than 4 degrees (yellow points). Furthermore, 4 of these pixels have slope angles equal to 0 from the DEM. These small angles are for practical effect equal to flat terrain. In this scenario the probabilistic forecast model is unable to predict any unstable state, even during a more serious rainstorm. However, the real occurrence of landslide events at these locations indicates further analysis is necessary. In this case, the most probable cause of this situation is the generalization process associated with the resolution of the DEM. It is well known that increasing the size of the pixel tends to lower the estimated slope value, which in turn will raise the failure prediction rate of models with high dependence on accurate slope values. A straightforward solution to this problem is to further reduce the size of the pixel, which will in turn represent the real slope angle more accurately. This solution however will drastically increase the computing time. As reference, the current matrix dimensions of 2576×2704 (for 125 m pixel size) represent the limit for a regular workstation when the data is not partitioned.

There is still 8 prediction failures (marked by red dots) unexplained. These are considered to be related to other aspects of the probabilistic forecasting model and unaccounted uncertainties. Detailed forecasting information about the landslide events in this study is listed in Table 4.

Table 4 Detailed forecasting analysis

| landslides | Successful predicted landslides | Failure to predict land- slides due to DEM imprecision | Failure to predict land- slides due to model imprecision | Failure rate |
|------------|------------------------------------|--|--|--------------|
| 176 | 159 | 9 | 8 | 9.7% |

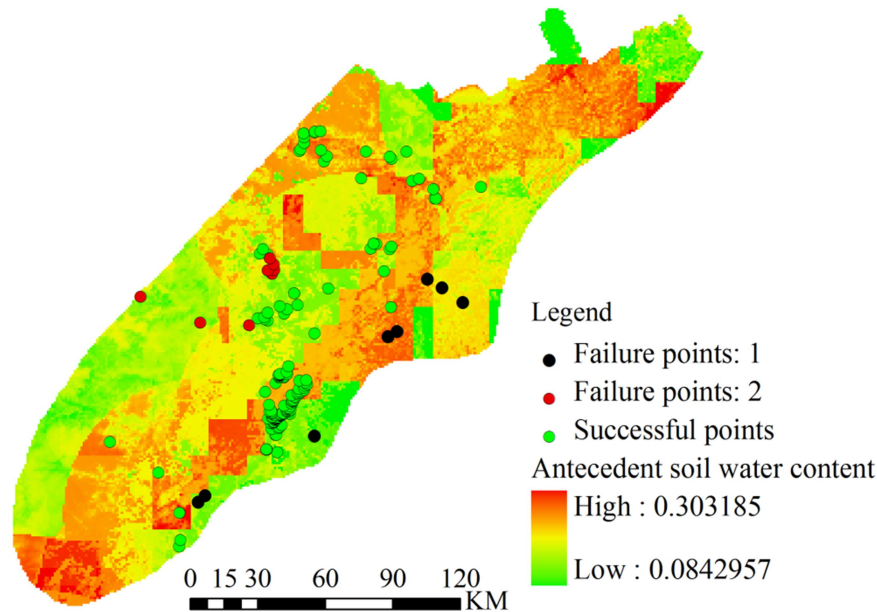
The false prediction (false positives) rate for the probabilistic forecast model is high. The Fig. 9 shows high warning degrees concentrated around Guangyuan City and Qingchuan County (marked by “red star” in Fig.9b), where landslide events did not occur. Looking at Fig. 3, the accumulative precipitation within Guangyuan City during the days of July 1st and 7th are 317.7 mm according to the local weather station. This implies initial soil water contents in the region close to saturation levels just before the forecasting time. Additionally, the cumulative precipitation predicted from the Doppler radar reached more than 470 mm in Guanyuan City. Under the action of such a combination of strong antecedent rainfall and forecasted rainfall, it is reasonable to expect high concentration of landslides (forecasted by the probabilistic model with different warning colors). Although the measured rainfall data for July 9th was not available for this study, indirect information (absence of report of landslides and other phenomena associated with heavy rainfall, even with notable initial soil water content levels) indicates the real precipitation on July 9th was much smaller than forecasted from Doppler radar. Adding the known tendency of Doppler radar forecasts to overestimate rainfall, it is reasonable to consider the precision of Doppler radar rainfall as a key factor influencing the high false prediction rates of the proposed probabilistic forecasting model.

5 Discussions

The general rule for the evolution of a slope from stability to failure is that the failure probability should increase as the rainfall process continues since increasing soil water content will decrease the suction matrix. This rule implies a forecasting result at 15:00 PM with more unstable pixels than the result at 6:00 AM. However, both of them are relatively close.

The distribution map of initial soil water content at 24:00 on July 8th, shown in Fig. 10, indicates significant effects of accumulated rainfall for landslide forecasting, the topsoil of some areas are even in saturated conditions (this means that only the topsoil was saturated rather than the whole soil layer). The total saturated pixels within

383 study region are 532.



384
385 Fig.10 Intial conditions for landslide forecasting

386 Under these initial conditions, the mechanism of the runoff-infiltration process indicates that significant
387 amount of precipitations will transform directly into runoff as the soil water content value of topsoil increases. In
388 this case study, these high levels of initial soil water content attributed to strong antecedent rainfalls leads to lower
389 variation rate of soil water content at pixel level. In this scenario, the variation of soil water content tends be gen-
390 tle even during long and intensive rain, while excess water contribute mainly to the runoff process. This chain of
391 events may explain the lack of clear evolution in the forecast in this particular study.

392 To further confirm this analysis, a new hydrological simulation was run in which the antecedent precipitation
393 is ignored. The initial soil water content of each pixel for landslide forecasting was directly assigned with the
394 residual soil water value according to the corresponding soil type (assuming a completely dry soil). All other pa-
395 rameters, including predicted rainfall from Doppler radar remained unchanged from the previous simulation. The
396 forecast results at 6:00 AM and 15:00 PM under these new conditions are shown in Fig. 11 and Table 5. It is easy
397 to observe differences between forecasting times, with quantity of unstable pixels at 15:00 PM larger than at 6:00
398 AM as expected. In this case, the low level of initial soil water content allows for strong infiltration process in the
399 topsoil, which in turn leads to high variation rates for soil water content in each pixel, reflected in the differences
400 of forecasting aligned with the expected evolution of the slope failure process.

401 Above analysis not only explain why there is not big difference between 6:00 AM and 15:00 PM forecasts dur-
402 ing a high intensive rainstorm. It also to stress the relevance of the initial soil water content (or the effective ante-
403 cedent rainfall) for any physically based landslide forecast model. A reliable method to calculate the initial soil
404 water content can significantly influence the results of landslide forecasting models.

405 Table 3 Quantity of pixels with warning information, without considering the influence of antecedent soil water content

| Warning colors | | Blue | Yellow | Orange | Red |
|----------------|----------|------|--------|--------|-----|
| pixel | 6:00 AM | 229 | 106 | 237 | 325 |
| count | 15:00 PM | 328 | 128 | 290 | 586 |

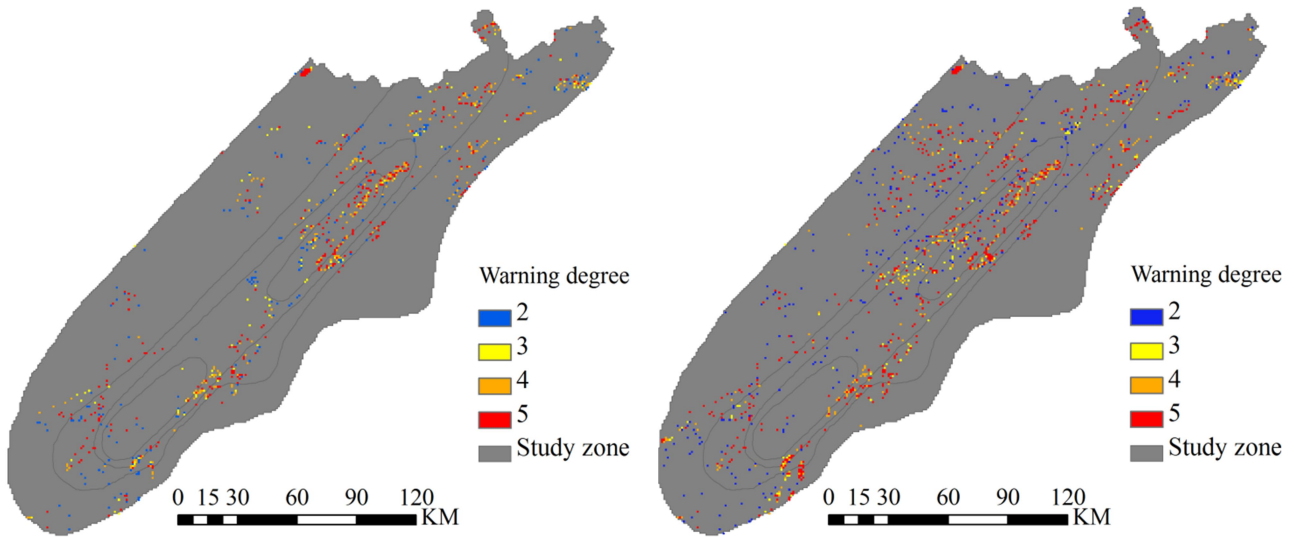


Fig.12 Forecasting results without considering the influence of the antecedent soil water content

Another issue is that most published physical models for landslide forecast such as the SLIP and TRIGRS models (Montrasio et al., 2011; Tsai and Chiang, 2012) overestimated the probability of landslide occurrence at regional scales. This proposed physics-based probabilistic forecasting model is also affected by this problem. From the point of view of input parameters, three key factors can lead to this high false prediction rate. (1) The soil mechanical parameters can only be obtained indirectly at regional scales, which greatly increase uncertainty. Consequently, it is impossible to guarantee the correspondence of the fixed mechanical values at pixel level with the actual values in nature, even using large intervals of soil mechanical parameters such as in this paper. Underestimating these values increase the probability to identify the corresponding pixel as unstable, which contribute to high false prediction rates. (2) The nature of DEM models implies that a pixel identified as unstable by a pixel based forecasting model may not really represent an unstable slope in nature. A slope may contain several pixels of which only a few are unstable, or more likely at regional scales, a pixel may include several slopes. In this scenario isolated unstable pixels can contribute to high false prediction rates. (3) The precision of short term rainfall forecasting is the last factor that can contribute to high false prediction rates. This is relevant in this study in which rainfall forecasts from Doppler radar overestimated the expected rainfall in some areas.

6 Conclusions

The extreme complexity of the landslide formation process conditions that even physics-based forecasting models are unable to model the slope instability with 100% of confidence. However, the uncertainty of some input variables (e.g., soil mechanical parameters) is responsible for a significant part of this situation. This research adopted a probabilistic approach to express this uncertainty using Monte Carlo simulation. A single parameter (the ratio P) was devised to couple the uncertain nature of input variables with shallow landslides forecasting. Furthermore, a regional physics-based probabilistic shallow landslide forecasting model was developed around this parameter. The proposed model does not eliminate uncertainty; it manages it by explicitly introducing it into the model expressing the forecast directly in probabilistic form. Our tests shown that this approach increases the forecast precision (true positives) in real conditions, which is cardinal to protecting the public from catastrophic consequences of shallow landslides and other associated disasters (such as debris flows).

It must be noted that the complexity of landslide forecasting is not limited to the uncertainty of physical soil properties, this research points to the initial soil water content as another key variable extremely difficult to identify accurately at regional scales. The model proposed in this paper implements a simulation of the hydrological processes occurring in the soil to estimate this value. Such simulation is time intensive, which is unfavorable for real world applications. Future research should focus in efficient methods for identification of soil water content at

438 regional scales, which is a difficult but worthy challenge.

439 The goal of developing this physics-based probabilistic forecasting model is to serve for regional landslide
440 disaster mitigation. Detailed resolution data, which in case of DEMs is readily available, are not always straight-
441 forward solutions for better forecasting results at this scale. In this case higher DEM resolution will improve the
442 efficiency of the model failure prediction rates at individual pixel level due to better slope representation. Howev-
443 er, it will also increase the time and resources required by the model to produce usable results. A balance point
444 between pixel-level precision and operational efficiency is required for the proposed model in order to make it
445 more suitable for regional operation.

446 **Acknowledgement:** This work was supported by Science and Technology Service Network Initiative (No:
447 KFJ-SW-STS-180), the Science and Technology Support Project of Sichuan Province (No. 2015SZ0214), the Risk
448 assessment on geohazards induced by extreme rainfall (CCSF201428), and hydrometeorological forecasting pro-
449 ject from National Meteorological Center of China Meteorological Administration.

450 Reference

- 451 Acharya, G., De, S.F., and Long, N.T.: Assessing landslide hazard in GIS: a case study from Rasuwa, Nepal. *Bull Eng. Geol. Environ*
452 65(1), 99 – 107, 2006.
- 453 Aleotti, P.: A warning system for rainfall-induced shallow failures, *Eng. Geol.*, 73, 247-265, 2004.
- 454 Apip, Kaoru Takara, Yosuke Yamashiki, Kyoji Sassa, Agung Bagiawan Ibrahim, and Hiroshi Fukuoka: A distributed hydrologi-
455 cal-geotechnical model using satellite-derived rainfall estimates for shallow landslide prediction system at a catchment scale,
456 *Landslides*, 7, 237-258, 2010.
- 457 Baum, R.L., Savage, W.Z., and Godt, J.W.: TRIGRS-a FORTRAN program for transient rainfall infiltration and grid-based regional
458 slopestability analysis, Virginia, US Geological Survey Open file report 02-424, 2002.
- 459 Baum, R.L., Savage, W.Z., and Godt, J.W.: TRIGRS-a FORTRAN program for transient rainfall infiltration and grid-based regional
460 slopestability analysis, Virginia, US Geological Survey Open file report 2008-1159, 2008.
- 461 Blondeau, F.: The residual shear strength of some French clays: measurement and application to a natural slope landslide, *Geologia*
462 *Applicata e Idrogeologia*, 8(1), 125–141, 1973.
- 463 Caine, N.: The rainfall intensity – duration control of shallow landslides and debris flows. *Geogr. Ann.* A62:23-27, 1980.
- 464 Cardinali, M., Galli, M., Guzzetti, F., Ardizzone, F., Reichenbach, P., and Bartoccini, P.: Rainfall induced landslides in December
465 2004 in Southwestern Umbria, Central Italy. *Nat. Hazards Earth Syst. Sci.*, 6, 237-260, 2006.
- 466 Chang, K., Chiang, S.H., and Lei, F.: Analysing the relationship between typhoon-triggered landslides and critical rainfall conditions,
467 *Earth Surf Process Land*, 33, 1261-1271, 2008.
- 468 Crosta, G.: Regionalization of rainfall thresholds: an aid to landslide hazard evaluation, *Environ. Geol.*, 35(2 – 3), 131 – 145, 1998.
- 469 Crosta, G.B., and Frattini, P.: Rainfall thresholds for triggering soil slips and debris flow. In: Mugnai A, Guzzetti F, Roth G (eds)
470 *Mediterranean storms. Proceedings of the 2nd EGS Plinius Conference on Mediterranean Storms.* Siena, Italy, pp 463 – 487,
471 2001.
- 472 Crosta, G. B. and Frattini, P.: Distributed modeling of shallow landslides triggered by intense rainfall, *Nat. Hazards Earth Syst. Sci.*, 3,
473 81–93, 2003.
- 474 Cruden, D.M., and Varnes, D.J.: Landslides types and processes. In: Truner AK, Schuster, R.L. (eds) *Landslides: investigation and*
475 *mitigation.* Transportation Research Board Special Report 247. National Acadmy Press, Washington, pp 36-75, 1996.
- 476 Cui, P., Yang, K., and Chen, J.: Relationship between occurrence of debris flow and antecedent precipitation: Taking the Jiangjia
477 Gully as an example, *China Journal of Soil and Water Conservation*, 1(1), 11-15, 2003. (in Chinese)
- 478 Dai, F.C., and Lee, C.F.: A spatiotemporal probabilistic modeling of storm-induced shallow landsliding using aerial photographs and
479 logistic regression, *Earth Surf Process Land*, 25, 527-545, 2003.
- 480 Davide, T., and David, R.: Estimation of rainfall thresholds triggering shallow landslides for an operational warning system, *Land-*
481 *slides*, 7: 471-481, 2010.

482 Fredlund, D.G., and Rahardjo, H.: Soil Mechanics for Unsaturated Soils. A Wiley-Interscience Publication, New York, USA, 1993.

483 Gao, K.C., Wei, F.Q., Cui, P., Hu, K.H., Xu, J., and Zhang, G.P.: Probability forecast of regional landslide based on numerical weather
484 forecast, Wuhan University Journal of Natural Sciences, 11(4), 853-858, 2006.

485 Iverson, R.M.: Landslide triggering by rain infiltration. Water Resources Research, 36, 1897-1910, 2000.

486 Jacob, M., Holm, K., Lange, O., and Schwab, J.W.: Hydrometeorological thresholds for landslide initiation and forest operation
487 shutdowns on the north coast of British Columbia, Landslides, 3(3), 228-238, 2006.

488 Jia, G.Y., Tian, Y., Liu, Y., and Zhang Y.: A static and dynamic factors-coupled forecasting model of regional rainfall-induced land-
489 slides: A case study of Shenzhen, Science in China Series E: Technological Sciences, 51(11), 164-175, 2008.

490 Lei, Z.D., Yang, S.X., and Xie, S.C.: Soil water dynamics, Beijing, Tsinghua University, 1988. (in Chinese)

491 Li, W.C., Lee, L.M., Cai, H., Li, H.J., Dai, F.C., and Wang, M.L.: Combined roles of saturated permeability and rainfall characteris-
492 tics on surficial failure of homogeneous soil slope, Eng. Geol., 153, 105–113, 2013.

493 Liu, D.L., Zhang, S.J., Yang, H.J., Zhao, L.Q., Jiang, Y.H., Tang, D., and Leng, X.P.: Application and analysis of debris-flow early
494 warning system in Wenchuan earthquake-affected area, Natural hazards and earth system science, 16, 483-496, 2016.

495 Montgomery, D.R., Dietrich, W.E.: A physically based model for the topographic control on shallow landsliding, Water Resources
496 Research, 30(4), 1153-1171, 1994.

497 Montgomery, D.R., Sullivan, K., and Greenberg, M.: Regional test of a model for shallow landsliding, Hydrological Process, 12,
498 943– 955, 1998.

499 Montrasio, L., Valentino, R., and Losi, G.L.: Towards a real-time susceptibility assessment of rainfall-induced shallow landslides on a
500 regional scale, Nat. Hazards Earth Syst. Sci., 11, 1927-1947, 2011.

501 Richards, L.A.: Capillary condition of liquids in porous mediums, Physics, 1, 318-333, 1931.

502 Raia, S., Alvioli, M., Rossi, M., Baum, R.L., Godt, J.W., and Guzzetti, F.: Improving predictive power of physically based rain-
503 fall-induced shallow landslide models: a probabilistic approach, Geosci. Model Dev., 7, 495-514, 2014.

504 Rossi, G., Catani, F., Leoni, L., Segoni, S., and Tofani, V.: HIRESSS: a physically based slope stability simulator for HPC applica-
505 tions, Nat. Hazards Earth Syst. Sci., 13, 151-166, 2013.

506 Salciarini, D., Godt, J.W., Savage, W.Z., Conversini, P., Baum, R.L., and Michael, J.A.: Modeling regional initiation of rain-
507 fall-induced shallow landslides in the eastern Umbria Region of central Italy, Landslides, 3(3), 181-194, 2006.

508 Schmidt, J., Turek, G., Clark, M.P., Uddstrom, M., and Dymond, J.R.: Probabilistic forecasting of shallow, rainfall-triggered land-
509 slides using real-time numerical weather predictions, Nat. Hazards Earth Syst. Sci., 8, 349-357, 2008.

510 Tang, C.: Activity tendency prediction of rainfall induced landslides and debris flows in the Wenchuan earthquake areas, Journal of
511 Mountain Science, 28(3), 341-349, 2010. (in Chinese)

512 Tsai, T.L., and Chiang, S.J.: Modeling of layered infinite slope failure triggered by rainfall, Environ. Earth Sci., 68(5), 1429-1434,
513 2012.

514 Van Genuchten: A closed form equation for predicting the hydraulic conductivity of unsaturated soils, Soil Science Society of Amer-
515 ica Journal 44, 892-898, 1980.

516 Varnes, D.J.: Slope movements types and process. In: Schuster, R.L., Krizeck, R.J. (eds) Landslides: analysis and control. National
517 Academy of Science, Washington, D.C., pp 11-30, 1978.

518 Wei, F.Q., Tang, J.F., Xie, H., and Zhong, D.L.: Debris flow forecast combined regions and valleys and its application, Journal of
519 Mountain Science, 22(3), 321-325, 2004. (in Chinese)

520 Wei, F. Q., Gao, K. C., Cui, P., Hu, K.H., Xu, J., Zhang, G., Bi, B.: Method of Debris Flow Prediction Based on a Numerical Weather
521 Forecast and Its Application, WIT Transactions on Ecology and the Environment, 90, 37–46, doi: 10.2495/DEB060041, 2006.

522 Wei, F.Q., Gao, K.C., Jiang, Y.H., Jia, S.W., Cui, P., Xu, J., Zhang, G.P., and Bi, B.G.: GIS-based prediction of debris flows and
523 landslides in Southwestern China//CHEN, C. L., MAJOR, J. J., Debris-Flow Hazards Mitigation: Mechanics, Prediction, and
524 Assessment. Rotterdam: Millpress Science Publishers, 479-490, 2007a.

525 Wei, F.Q., Xu, J., Jiang, Y.H., and Zhang J.: The system of debris flow prediction with different time and space scales. Journal of
526 Mountain Science, 25(5), 616-621, 2007b. (in Chinese)

527 Wieczorek, G.F., and Glade, T.: Climatic factors influencing occurrence of debris flows. In: Jakob M, Hungr O (eds) Debris flow
528 hazards and related phenomena. Berlin, Springer, pp325-362, 2005.

529 Wilkinson, P.L., Anderson, M.G., and Lloyd, D.M.: An integrated hydrological model for rain-induced landslides prediction. *Earth*
530 *Surf Process Land*, 27, 1285-1297, 2002.

531 Wu, W., and Sidle, R.C.: A distributed slope stability model for steep forested basins, *Water Resources Research*, 31(8), 2097– 2110,
532 1995.

533 Xu, J.J.: Application of a distributed hydrological Model of Yangtze River basin, Beijing: Tsinghua University, 2007. (in Chinese)

534 Yang, D.W., Herath, S., and Musiake, K.: A hillslope-based hydrological model using catchment area and width function, *Hydrolog-*
535 *ical Sciences Journal*, 47(1): 231-243, 2002.

536 Ye, J.H., Xi, Q.X., and Xia, W.R.: Handbook of rock mechanics parameters, Beijing, China Waterpower Press., 1991.

537 Zhang, S.J., Yang, H.J., Wei, F.Q., Jiang, Y.H., and Liu, D.L.: A model of debris flow forecast based on the water-Soil coupling
538 mechanism. *Journal of Earth Science*, 25(4), 757-763, 2014a.

539 Zhang, S.J., Wei, F.Q., Liu, D.L., Yang, H.J., and Jiang, Y.H.: A regional-scale method of forecasting debris flow events based on
540 water-soil coupling mechanism, *Journal of Mountain Science*, 11(6), 1531-1542, 2014b.

541 Zhang, S.J., Jiang, Y.H., Yang, H.J., and Liu, D.L.: A hydrology-process based method for antecedent effect rainfall determination in
542 debris flow forecasting, *Advance in Water Science*, 26(1), 35-43, 2015. (in Chinese)

543 Zhang, S.J., Wei, F.Q., Liu, D.L., and Jiang, Y.H.: Analysis of slope stability based on the limit equilibrium equation and the hydro-
544 logical simulation. *Journal of Basic Science and Engineering*, in Pres. (in Chinese)

545 Zhou, C.Y., Cen, S.X., Li, Y.Q., Peng, G.Z., Yang, S.Q., and Peng, J.: Precipitation variation and its impacts in Sichuan in the last 50
546 years, *Journal of Geographical Science*, 66(5), 619-630, 2011. (in Chinese)